# Output Power Limitations and Improvements in Passively Mode Locked GaAs/AlGaAs Quantum Well Lasers

Giuseppe Tandoi, Charles N. Ironside, *Senior, Member, IEEE*, John H. Marsh, *Fellow, Member, IEEE*, A. Catrina Bryce, *Fellow, Member, IEEE*

***Abstract*—We report a novel approach for increasing the output power in passively mode locked semiconductor lasers. Our approach uses epitaxial structures with an optical trap in the bottom cladding that enlarges the vertical mode size to scale the pulse saturation energy. With this approach we demonstrate a very high peak power of 9.8 W per facet, at a repetition rate of 6.8 GHz and with pulse duration of 0.71 ps. In particular, we compare two GaAs/AlGaAs epilayer designs, a double quantum well design operating at 830 nm and a single quantum well design operating at 795 nm, with vertical mode sizes of 0.5 and 0.75 μm, respectively. We show that a larger mode size not only shifts the mode locking regime of operation towards higher powers, but also produces other improvements in respect of two main failure mechanisms that limit the output power: the catastrophic optical mirror damage and the catastrophic optical saturable absorber damage. For the 830 nm material structure, we also investigate the effect of non-absorbing mirrors on output power and mode locked operation of colliding pulse mode locked lasers.**

***Index Terms*—High peak power laser, mode locked laser, non-absorbing mirrors, quantum well laser, sub-picosecond pulse generation.**

## I. Introduction

PASSIVELY mode-locked (ML) semiconductor lasers are sources of short optical pulses, particularly attractive for their low cost, small size and ease of pumping. GaAs/AlGaAs quantum well (QW) ML lasers operate in the 700-850 nm range, with several potential applications such as short-haul optical telecommunications, radio-over-fibre networks [1] and two-photon absorption microscopy [2]. While typical pulse durations are of 2-3 ps at repetition rates of a few 10-100 GHz [3-5], their use is limited by their low average output power, with typical values below 5 mW. As a result, the maximum peak powers rarely exceed 500 mW. Although great efforts have been made in the pulse-width reduction [6-7], similar average and peak powers have been reported in monolithic ML QW lasers operating at 1.3 and 1.55 μm, with the shortest reported pulses of the order of 1 ps and at frequencies up to ~50 GHz [8].

These power limitations are generally due to the passive mode locking mechanism itself, which relies on the self-formation of optical pulses from random intensity spikes occurring in the laser cavity, thanks to the pulse-shortening effect produced by the saturable absorber (SA). The SA is usually a reverse biased section of the laser cavity providing the necessary intensity-dependant absorption. This enhances intensity spikes with energies higher than the SA saturation energy over continuous wave (CW) radiation. With slow SAs (whose recovery time is longer than the pulse duration, which is the case for semiconductor SAs [9, 10]), dynamic gain saturation introduces net loss on the trailing edge of the pulse [9, 10]. For both the gain and SA sections of a semiconductor ML laser, the saturation energy can be defined as [11]

$$E_{g,\alpha}^{sat} = \frac{h\nu A_{g,\alpha}}{d(g,\alpha)/dN_{g,\alpha}} = \frac{h\nu}{d(g,\alpha)/dN_{g,\alpha}} \frac{wd}{\Gamma}, \quad (1)$$

where $h$ is Planck's constant, $\nu$ the optical frequency, $d(g,\alpha)/dN_{g,\alpha}$ the differential gain or absorption (with $N$ being the carrier density), $A_{g,\alpha}$ the cross sectional area of the laser mode, $w$ the waveguide width, $d$ the well thickness and $\Gamma$ the optical confinement in the QWs. Equation (1) shows that the laser epistructure design plays a crucial role in the final output power performance of the ML device through the geometrical parameter $wd/\Gamma$ ($d/\Gamma$ represents the effective vertical mode size). While in conventional semiconductor lasers the pulse gain saturation energies are generally small and in the 0.3-3.0 pJ range [8], recent experiments have shown that, in a slab coupled optical waveguide geometry, these can be scaled up to 30-100 pJ, by increasing the optical mode area and reducing the overlap of the optical mode with the active region [12]. Average output powers of 200-250 mW and pulse-widths of 5-6 ps (peak power close to 4 W) have been reported from devices with a cavity length of around 8-10 mm with this waveguide design [12-14], at repetition rates of 4-7 GHz. With a similar waveguide structure, 10 ps wide pulses at a peak power of 5.8 W were achieved at 4.29 GHz in 2006 [15].

Sub-picosecond pulses are usually more easily generated in quantum dot (QD) and quantum dash ML lasers with the short

Manuscript received September 19, 2011. This work was supported in part by the Engineering and Physical Sciences Research Council (EPSRC) under Grant EP/E065112/1.

G. Tandoi is with the School of Engineering, University of Glasgow, Glasgow, UK. (e-mail: Giuseppe.Tandoi@glasgow.ac.uk).

C. N. Ironside, is with School of Engineering, University of Glasgow, Glasgow, UK (e-mail: Charles.Ironside@glasgow.ac.uk).

J. H. Marsh, is with the School of Engineering, University of Glasgow, Glasgow, UK (e-mail: John.Marsh@glasgow.ac.uk).

A. C. Bryce is with the School of Engineering, University of Glasgow, Glasgow, UK (e-mail: Catrina.Bryce@glasgow.ac.uk).

pulses bringing a further increase in the peak power. Compared to QW devices, QD lasers are particularly advantageous for use as sources of ultrashort Fourier-limited pulses and as high power laser sources [16-18], thanks to their low threshold currents, broad gain spectrum, reduced linewidth enhancement factor, low saturation energy, weak quantum confined Stark effect (QCSE) and fast recovery times [16-18]. In standard QD ML lasers, pulses not shorter than 1-3 ps are typically achieved and with average powers not higher than around 50 mW [16-18]. However, using a combination of QD materials and flared waveguide geometries, implemented to both increase the output power and to enhance saturation within the absorber, Fourier-limited pulses as short as 360 fs have been reported, with peak powers from hundreds of mW up to few W [19-22]. A record peak power of 15 W was achieved in a gain-guided/tapered QD device [24]. Sub-picosecond pulses have also recently been reported from quantum dash ML lasers without flared geometries [25, 26].

In this work, we investigate a novel approach for increasing the output power from QW semiconductor ML devices, based on the use of high $d/\Gamma$ laser epistructures for the scaling of the pulse saturation energy, and demonstrate a very high peak power of 9.8 W per facet. In particular, we compare two GaAs/AlGaAs epilayer designs operating at around 830 and 795 nm and with $d/\Gamma$ ratios of 0.5 and 0.75 μm, respectively. Moreover, we show that the $d/\Gamma$ parameter not only shifts the mode locked regime of operation towards higher powers, but also produces other benefits in respect of two main failure mechanisms that limit the output power from semiconductor passively ML lasers: catastrophic optical mirror damage (COMD) [27, 28] and catastrophic optical saturable absorber damage (COSAD). As will be shown, in both COMD and COSAD permanent damage is produced in the part of the laser where a positive feedback loop, involving an increase in local temperature and a thermal increase in local absorption, is triggered by high optical powers. This paper is thus organized as follows. The two laser structures and device geometries are described in Section II, including details of the device fabrication steps. Section III presents the material gain and absorption measurements, used for analysing the operating regimes of the fabricated ML devices. Sections IV and V report results from the 830 and 795 nm ML devices, respectively. The conclusions are given in Section VI.

## II. Material and Device Structures

In this work, two GaAs/AlGaAs laser epistructures grown by metal organic chemical vapor deposition (MOCVD) have been considered. Their designs are similar to those discussed in [26, 27] and have been optimized for high power applications, such as laser print heads [29], for pumping $Er^{3+}$-doped fiber amplifiers (EDFA) [30] or Nd:YAG solid state lasers.

The first structure comprises two 4.4 nm thick GaAs QWs spaced by a 9 nm thick $Al_{0.2}Ga_{0.8}As$ barrier. These are sandwiched between two 120 nm thick undoped layers forming a graded index separate confinement heterostructure (GRIN-SCH). The designed emission wavelength is around 830 nm. A 1.9 μm thick $Al_{0.32}Ga_{0.78}As$ layer with graded *p*-doping is used as *p*-cladding and a 3 μm thick $Al_{0.32}Ga_{0.78}As$ layer with graded *n*-doping is used as *n*-cladding. The *n*-cladding also incorporates a 0.7 μm thick optical trap layer with an Al mole fraction graded from 0.32 to 0.29 and spaced away from the GRIN-SCH waveguide. The second laser material consists of an active region with a 7 nm thick AlGaAs QW (with Al mole fraction designed for emission at 793 nm) and two 7 nm thick $Al_{0.35}Ga_{0.65}As$ barriers, sandwiched between two GRIN-SCH waveguide layers with thicknesses of 90 nm and 60 nm, the top and the bottom one, respectively. The *p*-doped $Al_{0.65}Ga_{0.35}As$ and the *n*-doped $Al_{0.55}Ga_{0.45}As$ cladding layers are 1 and 3.5 μm thick, respectively, again with graded doping profiles. The lower cladding also contains a 0.37 μm thick optical trap, with Al mole fraction graded from 0.55 to 0.52. In both structures, the optical trap introduces several benefits to high power operation. The trap reduces the vertical far-field divergence, by enlarging the vertical mode profile, and improves single transverse mode operation, by increasing the loss for transverse modes higher than the fundamental [27, 28]. This effect is enhanced in the 793 nm material by the asymmetric cladding design.

For the 830 nm structure, an optimal waveguide 1.9 μm deep and a 2.5 μm wide was found for single mode operation and with an optical confinement of 0.0083 per well. For the 793 nm structure, an optimal waveguide 1.2 μm deep and 3 μm wide was determined, with a $\Gamma$ of 0.0093. Such low values of $\Gamma$ result in $d/\Gamma$ ratios of 0.5 and 0.753 μm, respectively for the 830 and 795 nm lasers, higher than those of more conventional laser structures [27, 28]. Moreover, the 793 nm structure presents an effective mode area of 2.26 $\mu m^2$, which is around 70% higher than that (1.34 $\mu m^2$) calculated for the 830 nm material. A high $d/\Gamma$ ratio is beneficial in high power lasers as it reduces the power density at the laser facet and thus the occurrence of COMD [27, 28]. In standard uncoated ridge waveguide lasers under CW pumping, a COMD power limit of 50 mW (~37 MW/$cm^2$) was found for the 830 nm material, while COMD-free powers higher than 90 mW (~40 MW/$cm^2$) were measured for the 793 nm lasers. A scanning electron microscope (SEM) photograph of the facet of an 830 nm laser damaged by COMD is shown in Fig. 1 (a), while in Fig. 1 (b) the computed mode intensity profile is plotted for comparison.

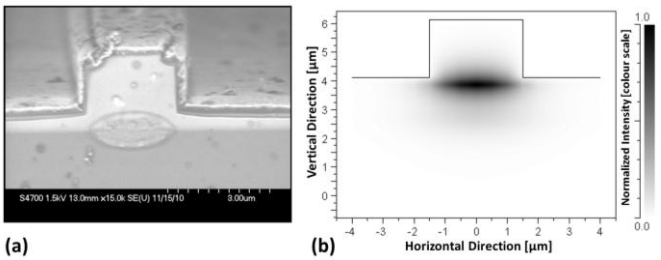


Fig. 1. (a) SEM photograph of the facet of an 830 nm laser damaged by COMD. (b) Plot of the computed mode intensity profile relative to a 1.9 μm deep and a 2.5 μm wide ridge waveguide in the 830 nm laser material.

A high $d/\Gamma$ ratio is also desired in passive ML laser diodes as it increases the saturation energy of the gain and SA sections, thus allowing the ML operation to occur at higher powers. Moreover, the reduced optical overlap reduces self phase modulation (SPM) for the same energy in the pulse, thus

allowing for shorter pulses to be generated.

The ML devices were fabricated using electron-beam lithography and dry etching steps. The ridge waveguides were formed by dry etching the AlGaAs layers using $SiCl_4$ in a reactive ion etching (RIE) system. The sample was then covered with a 600 nm thick layer of silica providing electrical isolation and the contact windows were opened on top of the waveguides. The SA and gain contact pads, separated by 10 μm long gaps were defined by lift-off processing. The highly doped GaAs cap layer was also dry etched in the gap regions to improve the isolation between the contact pads (with measured inter-contact resistances of around 5 kΩ).

## III. Gain and Absorption Measurements

Ridge waveguide lasers with multiple contacts were fabricated for measuring the gain and absorption spectra of the 830 nm material using the multisection technique described in [31]. The acquired data are used in this paper to analyze the operating regimes of the ML lasers under investigation. Figure 2(a) shows the measured gain spectra for different injection current densities, for both transverse electric (TE) and transverse magnetic (TM) polarizations. The intrinsic loss is estimated from the crossing points of the TE and TM gain curves (4.9 $cm^{-1}$). Figure 2 (b) shows the measured absorption spectra for different reverse voltages. A QCSE shift of around

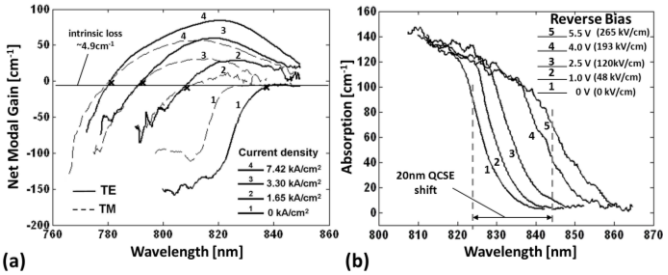


Fig. 2. (a) Plot of TE (continuous line) and TM (dashed line) modal gain spectra, for different injection current densities. The horizontal line gives the intrinsic loss of the material, found from the crossing points of the TE and TM gain curves. (b) TE absorption spectra for different reverse bias voltages. A wavelength shift of 20 nm of the spectrum is obtained with a reverse voltage of 5.5 V (265 kV/cm), due to QCSE. The absorption edge is measured as the wavelength for which the derivative $d\alpha/d\lambda$ is maximum.

20 nm was achieved with a reverse bias of 5.5 V (~265 kV/cm). Figures 3(a) and (b) plot the TE modal gain peak and peak wavelength as function of current density, respectively. In Fig. 3(b), it can be seen that the gain peak abruptly shifts from the lowest electron-heavy hole transition towards the

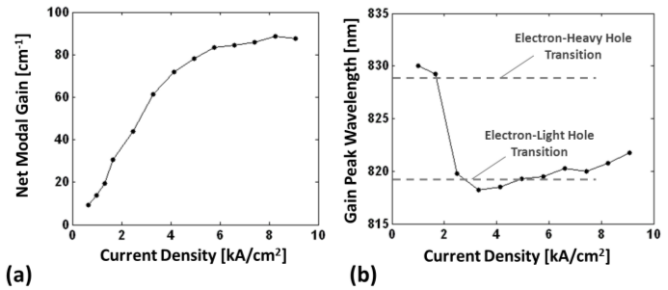


Fig. 3. (a) Modal gain peak versus current density obtained from the multisection measurements. (b) TE gain peak wavelength as function of current density. The TE gain peak moves from around 830 nm (electron-heavy hole transition) at low current densities towards around 820 nm (electron-light hole transition).

electron-light hole transition, as the current density is increased from 2 to 3 $kA/cm^2$. This abrupt gain peak shift plays an important role in the output power performance of our ML lasers, as it will be shown in next section.

## IV. 830 nm Mode Locked Lasers

In the 830 nm material, 3.7 mm long ML devices were fabricated with a single 222 μm long SA placed in the middle of the cavity, in order to provide colliding pulse mode locking (CPM) operation. The CPM regime is characterized by the emission of pulses at a repetition rate that is twice the Fabry-Pérot (FP) cavity round-trip frequency (~2×10 GHz). The CPM configuration is also beneficial as it allows the SA to be positioned away from the laser facets, where it would otherwise facilitate the occurrence of COMD [5]. For some devices, 150 μm non-absorbing mirrors (NAMs) were fabricated at each facet of the laser, as shown in the schematic in Fig. 4.

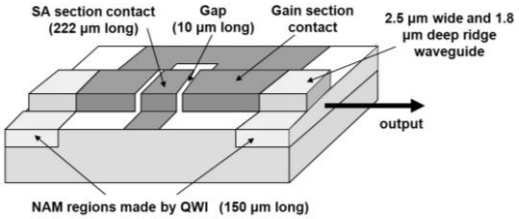


Fig. 4. Schematic of a CPM device with NAMs on both facets. Devices without NAMs have the same cavity length, but the gain section is extended to the facets.

NAMs are sections of the laser left unpumped in order to decrease the local carrier concentration, which is the main source of COMD [32]. A bandgap shift was produced selectively in the NAM regions by using a sputtering induced disordering (SID) quantum well intermixing (QWI) technique similar to that described in [33]. With this technique, a bandgap wavelength shift of around 62 nm was deduced from photoluminescence (PL) measurements. The bangap shift allows for a reduction of the thermally induced absorption at the facet and thus an increase in the COMD limit of around 40%, compared to the devices without NAMs, as shown in the light-current (*L-I*) curves in Fig. 5. Fig. 5 also shows a decreased slope efficiency in the devices with NAMs, due to their shorter gain section. In both devices, as will be shown, ML operation was found to occur at output powers below the COMD limit and a failure mechanism different from COMD

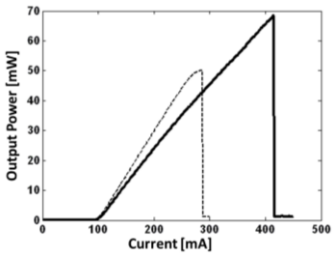


Fig. 5. *L-I* curves for 3.7 mm long CPM devices with 222 μm long SAs forward biased, with (solid line) and without (dashed line) NAMs.

was observed at such lower powers.

A further test included the measurement of the *L-I*s for

several values of SA reverse bias. The results are shown in Figures 6(a) and (b). The output power was measured for the

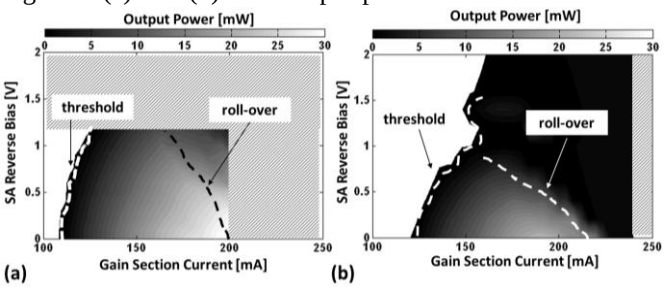


Fig. 6. Map of output power as function of the gain section current and of the SA reverse bias of 3.7 mm long CPM devices, without (a) and with (b) 150 μm long NAMs on both facets. The gain current step is 4 mA while the SA voltage step is 0.1 V. No data are available for the dotted-grey areas.

NAM device for gain currents $I_g$ between 100 and 240 mA, in steps of 4 mA, and SA reverse voltages $V_{SA}$ between 0 and 2 V, in steps of 0.1 V. The non-NAM device was instead tested for $I_g$ between 100 and 200 mA, in steps of 4 mA, and $V_{SA}$ between 0 and 1.2 V, in steps of 0.1 V. However, they are plotted in the same range for better comparison. The limitations shown in Fig. 6 in terms of maximum $I_g$ and maximum $V_{SA}$ were the result of failure of the devices due to damage of the SA. The reason was investigated in this work and will be explained in more detail later in this Section. However, it can be anticipated that, when a high optical power is absorbed by the SA, a high photocurrent is generated in the SA (which is under reverse bias), causing catastrophic damage of the SA. The SA failure was recognizable from the *p-n* junction breakdown, which prevented, after the damage, any current injection in the SA when forward biased. Moreover, this damage also caused the failure of the whole device, which did not lase after the SA degradation. This could also be observed through an optical microscope during device operation, because, before the failure, some red light could be seen along the whole gain section length, while, after failure, around 300 μm of the gain section on either sides of the SA no longer luminesced, indicating the damage to these portions of the gain section as well. This is similar to what is observed near the facets in the case of COMD. Another feature of the recorded *L-I*s is the output power roll-over occurring at relatively high currents. The roll-over power decreases with higher SA reverse voltages. As will be seen later in this section, this behavior significantly affects the laser regimes of operation.

In order to evaluate the range of mode locking, the RF spectrum was recorded for several values of $I_g$ and $V_{SA}$. The RF spectrum revealed the presence of peaks around 19.75 GHz, corresponding to twice the round-trip frequency, as expected in CPM operation. The RF peak amplitude (over the noise floor) is mapped as function of $I_g$ and $V_{SA}$ for both non-NAM and NAM devices in Figures 7 (a) and (b), respectively. These maps represent the range of CPM operation, as the emission of pulses was confirmed in this range through autocorrelation measurements. Both NAM and non-NAM devices have the highest RF peak at around $I_g$ = 200-210 mA and $V_{SA}$ = 0.3 V, but this is stronger (22 dB over the noise floor compared to 17 dB) and narrower (230 kHz compared to

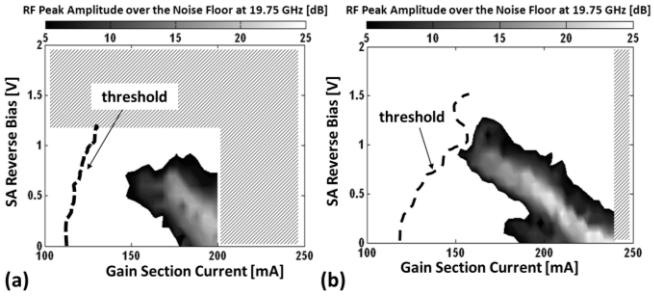


Fig. 7. Map of the 19.75 GHz RF peak amplitude over the noise floor, as a function of the gain section current and of the SA reverse bias of 3.7 mm long CPM devices, without (a) and with (b) 150 μm long NAMs on both facets. The gain current step is 4 mA while the SA voltage step is 0.1 V. No data are available for the dotted-grey areas.

160 kHz) in the device with NAMs, as we reported in [34].

The optical spectrum within the range of mode locking has a -3 dB width between 0.2 and 0.55 nm and is slightly larger for the NAM devices. Figure 8 shows the corresponding optical spectrum for both devices, where the mode spacing $\Delta\lambda$ doubles from that of the FP cavity $\Delta\lambda_{FP}$, confirming CPM operation. The optical bandwidth $\Delta\nu$ is 0.55 nm (0.24 THz) for the device with NAMs, while for the devices without NAMs it is about 0.5 nm (0.22 THz), under the optimum mode locking conditions.

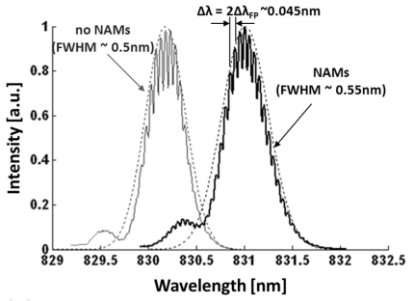


Fig. 8. Optical spectra under optimum CPM operation for NAM and non-NAM devices, where the FWHM is equal to 0.55 and 0.5 nm, respectively (considering Gaussian envelopes).

The emission of pulses was confirmed through two-photon absorption (TPA) autocorrelation measurements [35]. In [34] we reported the measured interferometric autocorrelation traces and the deduced pulsewidths of 1.84 ps (assuming a Gaussian pulse shape) for the device with NAMs and of 2.04 ps for the device without NAMs, under optimum mode locking. These values confirm that the pulses are nearly transform-limited for both devices. In this regime, the average output powers are 17 mW and 27 mW (corresponding to 462 mW and 675 mW peak powers) in devices with and without NAMs, respectively. The ~10% smaller pulsewidth of the laser with NAMs is consistent with the ~10% wider bandwidth of the optical spectrum. The shorter length (~10%) of the pumped section is also believed to reduce the non-linear phenomena and dispersive effects that usually contribute to broaden the pulses [36]. Furthermore, according to the work of Lau and Paslaski [9, 10] and to that reported in [15], improved ML operation is expected in device geometries with higher steady state gain, which also benefit from higher gain bandwidth and lower differential gain $dg/dN$ (advantageous for satisfying Equation (3) in [16]). In reference [16], although

not directly related to the pulse-width, steady state gain and differential gain are compared for different cavity designs and related to the shorter pulse-width measured in ML lasers with passive sections. In reference [16], it is also suggested to approximate the qualitative form of dependence of $dg/dN$ as a function of the carrier density $N$ (a material parameter typically not available as in our case), with the derivative $dg/dJ$ of the gain as function of the current density $J$. The values of $g$ and $dg/dJ$ have been estimated at 830 nm from the gain curves reported in Section III and are 10.93 $cm^{-1}$ and $25.49x10^{-3}$ cm/A for NAM devices, and 9.98 $cm^{-1}$ and $25.67x10^{-3}$ cm/A for non-NAM devices. Thus, reduced pulse-widths are obtained consistently with the better mode locking conditions provided by the higher (~10%) steady-state gain of the devices with passive sections, similarly to the reports in [16, 36]. Moreover, the reduction in pulse-width $\tau_p$ is also consistent with the reduction in RF peak power and width $\Delta\nu_{RF}$ observed in devices with NAMs. A dependence $\Delta\nu_{RF}/\tau_p^2$=const has been also theorized and reported in [37].

In both NAM and non-NAM lasers, a range of relaxation oscillations in the self-pulsation (SP) regime was observed from the recorded RF spectra. In this regime of operation, lasers usually emit broad pulses (several tens of ps) at a frequency lower than the cavity round-trip repetition rate and related to the carrier lifetime in the laser gain section [5, 10]. In our case, the RF peaks associated with the SP regime were in the range of 1-5 GHz (main peak at around 1 GHz). The SP peak amplitude (over the noise floor) is mapped as function of $I_g$ and $V_{SA}$ for both non-NAM and NAM devices in Figures 9(a) and (b), respectively.

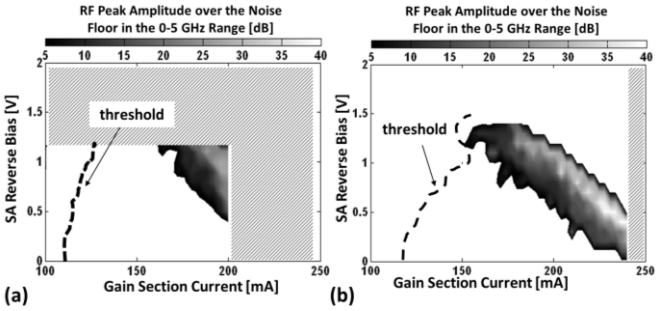


Fig. 9. Map of the SP peak amplitude over the noise floor, as function of the gain section current and of the SA reverse bias of 3.7 mm long CPM devices, without (a) and with (b) 150 μm long NAMs on both facets. The gain current step is 4 mA while the SA voltage step is 0.1 V. No data are available for the dotted-grey areas.

Comparing Figures 7 and 9, one can deduce that, for a given SA bias, the SP regime occurs at a gain current slightly higher (about 20-30 mA) than the value for best ML operation, preventing mode locking at higher currents and thus higher powers, similar to previous reports [5]. An abrupt jump from one regime to the other was observed when changing the current, with a small region of overlap between the two. Associated with the onset of SP, an abrupt decrease in the peak wavelength was visible in the optical spectrum, as shown in Figures 10(a) and (b), where the peak wavelength is mapped as function of $I_g$ and $V_{SA}$. From these plots one can see that when the current is increased, for a given SA bias, the optical spectrum peak moves towards higher wavelengths

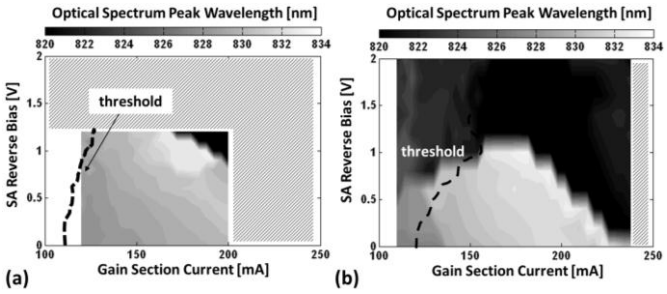


Fig. 10. Map of the peak wavelength as function of the gain section current and of the SA reverse bias of 3.7 mm long CPM devices, without (a) and with (b) 150 μm long NAMs on both facets. The gain current step is 4 mA while the SA voltage step is 0.1 V. No data are available for the dotted-grey areas.

compared to the threshold value, up to around 832 nm. Above this point, the peak abruptly jumps to around 822 nm. This behavior is similar in NAM and non-NAM devices, the only difference being the current at which the abrupt jump occurs. Furthermore, the strongest SP corresponds to the region of low output power in the $I_g$-$V_{SA}$ maps in Fig. 6.

The different regimes of operation are summarized in Fig. 11(a) for the device with NAMs. In Fig. 11(b), examples of the recorded optical spectra in the CW, ML and SP regimes are reported for $V_{SA}$ = 0.3 V. Output power and SA photocurrent are plotted as function of the gain section current, for $V_{SA}$ = 0.3 V, in Fig. 11(c). The roll-over in the *L-I* curve of Fig. 11(c) corresponds to the occurrence of the ML regime. Above this point the output power decreases abruptly due to the high current photo-generated in the SA. Figures 11(d) and (e) show the RF spectra under the strongest ML and SP operation, respectively. As seen in Fig. 11(c), the SA photocurrent increases linearly with increasing gain section

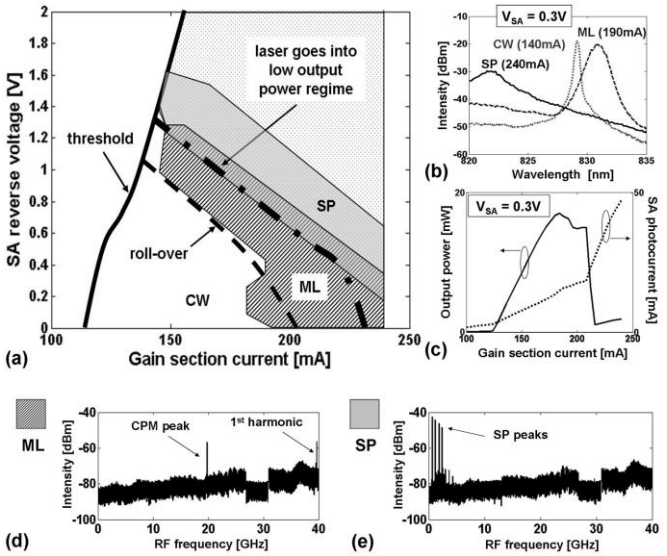


Fig. 11. (a) Map of regimes of operation of the device. (b) Examples of the optical spectra in the CW, ML and SP regimes for $V_{SA}$ = 0.3 V. (c) Plot of output power and SA photocurrent as function of the gain section current, for $V_{SA}$ = 0.3 V. The ML regime is associated to the roll-over in the LI curve. Above this point, the output power decreases abruptly due to the high current photo-generated in the SA. Catastrophic damage of the SA occurs for SA currents higher than 50 mA (~10 $kA/cm^2$). In (d) and (e) the RF spectra under strongest ML and SP operation are reported, respectively. All the plots (a)-(e) refer to the device with NAMs.

current (and thus with increasing optical power in the cavity). This remains true until a certain value of output power is reached, above which the SA photocurrent starts to increase more rapidly with power, forcing the laser to switch regime of operation. One possible explanation is that, when high optical powers are absorbed by the SA, the high SA photocurrent density heats the SA itself, reducing its bandgap. The red-shifted SA will thus absorb more at the lasing wavelength, with a consequent decrease in the laser output power and further increases in the SA bandgap red-shift and temperature. This mechanism, apart from producing the output power roll-over, caused the catastrophic damage of several devices, when the SA photocurrent was not kept below a certain limit (in this case around 50 mA - 9.4 kA/cm$^2$). The effect of the SA red-shift is illustrated in Fig. 12, where the spectra of laser gain and total cavity losses are plotted. The spectrum of the gain-length product $g(\lambda, I_g)\times L_g$ is indicated with black solid lines in Fig. 12, while the total cavity loss is indicated with grey dashed lines. The total loss is given by the sum $\alpha_{MIRR}L + \alpha_i L + \alpha_{SA}L_{SA}$, where $\alpha_{MIRR}$ is the mirror loss given by $[1/L] \times ln[1/R]$ ($R$~0.3 is the mean facet reflectivity), $\alpha_i$ the intrinsic loss, $L$ the cavity length, $\alpha_{SA}$ the SA absorption and $L_{SA}$ the SA length. These spectra represent the single pass gain or loss encountered in the laser cavity by the optical beam and are obtained from the multisection measurements discussed in Section III. All the grey dashed curves refer to the absorption spectrum in the case of $V_{SA}$ = 0.3 V, but with different wavelength shifts. Three different situations are considered. The first is when the laser is at threshold ($I_{th}$) and the SA is not heated significantly, thus referred to as 'cold'. In this situation, the gain spectrum clamps as the carrier density clamps at its threshold value. The point where the gain spectrum crosses the loss spectrum corresponds to the threshold wavelength $\lambda_{th}$ = 830 nm. As soon as the gain current is increased, the power within the cavity increases, producing a redshift in the SA bandgap. As an example for the second situation, a shift of 3 nm is considered in Fig. 12. This shift forces the gain spectrum to red-shift in order to compensate for the increased loss. Therefore, the optical spectrum peak wavelength increases accordingly (as confirmed by the data reported in Fig. 10). When the optical power in the laser is enough to produce a SA shift of around 6-7 nm, its effect becomes significant. In this condition, as shown in Fig. 12, the threshold wavelength moves to ~822 nm, where the SA absorption is significantly high. The increased SA absorption and reduced optical power make the SA itself more difficult to bleach, giving rise to relaxation oscillation SP regimes [38], as confirmed by the data in Fig. 9.

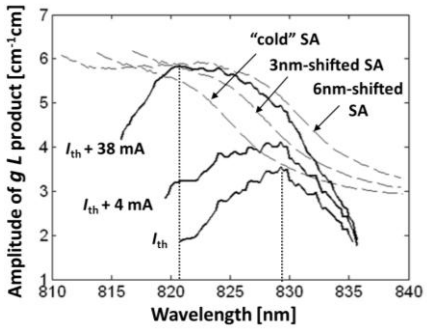


Fig. 12. Plot of the spectrum of the gain-length product $g(\lambda, I_g)L_g$ (black solid curves) and of the total cavity loss (grey dashed curves), given by the sum $\alpha_{MIRR}L + \alpha_i L + \alpha_{SA}L_{SA}$. Both gain and absorption data are taken from multisection measurements results described in Section III. All the grey dashed curves refer to the SA absorption spectrum for $V_{SA}$ = 0.3 V, but with different wavelength shifts, related to the power in the laser cavity. At threshold (gain curve indicated with current $I_{th}$), the SA is referred to as "cold" because the power in the cavity is relatively low and the SA is not particularly heated (low SA current photogenerated). The gain and the absorption curves cross each other at $\lambda_{th}$ = 830 nm. When the gain current is increased, also the optical power and the SA photocurrent increase. The heated SA red-shifts and the gain curve red-shifts accordingly, in order to compensate for the larger loss. The threshold current thus increases and the slope decreases accordingly. A 3 nm SA red-shift produces a threshold current increase of 4 mA and forces an operating wavelength of 831 nm, while a 6 nm SA red-shift produces a threshold current increase of 38 mA, forcing an operating wavelength of 822 nm.

The SA bandgap shrinkage can lead to a thermal run-away and thus to the catastrophic damage of the SA itself. As this mechanism is similar to COMD, it is reasonable to believe that the maximum optical power up to which a laser with an SA can be operated is not far from the COMD limit, around 50 mW in our case. This is in good agreement with what was observed from the devices damaged during the test due to COMD. For these devices, the failure occurred at gain currents higher than 250 mA, where the optical power for a fully forward biased device is close to 50 mW. Finally, an indicative estimation of the SA temperature can also be made. From the gain and absorption spectra analysis illustrated in Fig. 12, a SA red-shift of at least 6-7 nm was estimated in the case of the laser switching from ML to SP. Considering a bandgap wavelength temperature dependence of 0.3 nm/K [39], a temperature increase of 20-23 K can be associated to the 6-7 nm SA red-shift. With this SA shift, as shown in Fig. 12(c), a SA photocurrent of 20 mA is produced. In this condition, the SA photocurrent increases very quickly with increasing optical power. Moreover, as the SA temperature rise is proportional to the power dissipated in the SA itself, which is in turn proportional to $I_{SA}^2$, it is reasonable to expect at least a quadratic dependence of the temperature as function of SA photocurrent (also confirmed in [40] for facet temperature increases due to optical absorption). Considering destructive SA currents higher than 50 mA, SA temperatures increases of around 130 K can be estimated, in reasonable agreement with reported temperature variations leading to COMD in GaAs/AlGaAs lasers [41].

## V. 795 nm Mode Locked Lasers

As observed in Section III, high power mode locking operation was limited in the 830 nm devices by the occurrence of SP operation of the laser, associated with the high absorption regimes of the SA. COMD occurred at around 50 mW, but ML operation was limited to lower power levels (17-27 mW). This was due to the catastrophic damage of the SA produced by the high current densities (destructive when higher than ~10 kA/cm$^2$) induced by the absorption of high optical powers (of the same order of the COMD power). For

this reason a 795 nm epistructure with a 70% higher $d/\Gamma$ was considered, as already described in Section II. In Section II, it was shown that the higher $d/\Gamma$ improved significantly the COMD power limit, thanks to the enlarged mode profile and reduced optical confinement. Figures 13(a) and (b) show the computed TE mode profile for the designed ridge waveguide

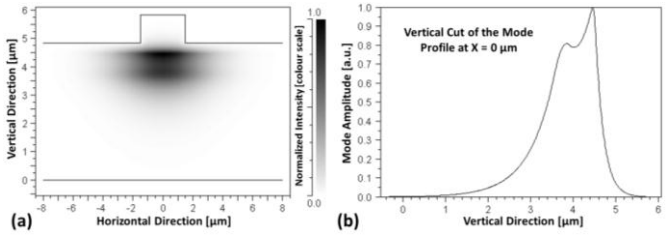


Fig. 13. (a) Computed TE mode profile for a 3 μm wide and 1.2 μm deep ridge waveguide. (b) Vertical cut of the computed mode profile.

and the vertical cut of the computed mode profile.

In this material structure, 5.69 mm long ML devices were fabricated with a 227 μm long SA at the facet. An improvement in the output power, compared to the 830 nm devices, was observed also when reverse biasing the SA, as shown in the $I_g$-$V_{SA}$ map in Fig. 14(a). A maximum power of 60 mW was measured in the biasing range considered. Despite of the increased output power, the SA photocurrent remained relatively small (maximum 25 mA - 3.67 kA/cm$^2$), compared to the 830 nm CPM devices (3 times higher with approximately the same SA length) described in Section III, as

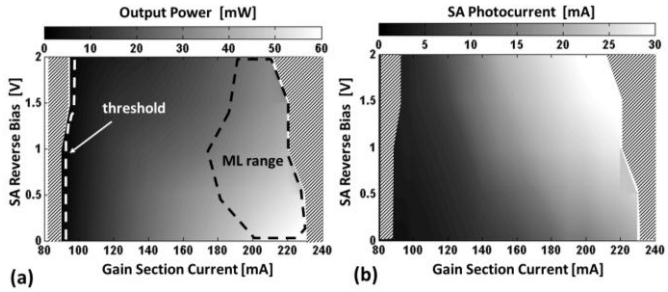


Fig. 14. Map of (a) output power and (b) SA photocurrent, as function of gain section current and SA reverse voltage. The gain current step is 10 mA while the SA voltage step is 0.5 V. No data are available for the dotted-grey areas.

shown in Fig. 14(b). The reduced photocurrent and thus reduced sensitivity to optical damage further confirms the benefits of the larger mode profile and smaller number of wells of the 793 nm laser structure for high power ML operation.

The ML operation range in terms of gain current and SA voltage was again assessed by measuring the RF spectrum. From these measurements, the RF peak power (at a frequency of around 6.84 GHz) was extracted and is plotted in Fig. 15(a). As shown, the highest (25 dB over the noise floor) RF peak occurs for $I_g$ = 210 mA and $V_{SA}$ = 0.5 V. The optical bandwidth is about 1.5 nm at $I_g$ = 210 mA and $V_{SA}$ = 0.5 V, where the highest RF peak occurs. The improved SA resilience to optical power in this material may also be responsible for the improved optical spectrum stability. The peak wavelength remains relatively unchanged when varying the gain current, while it decreases when increasing the SA reverse bias. The peak wavelength is plotted as function of SA bias and for $I_g$ in the range 200-220 mA in Fig. 15(b).

In Figures 16(a) and (b), the RF and optical spectra of the device under optimum ML conditions ($I_g$ = 210 mA and $V_{SA}$ = 0.5 V) are reported. Under the optimum ML conditions, the autocorrelation was also recorded, confirming the emission of sub-picosecond pulses (0.71 ps) at 6.86 GHz (around 146 ps), as shown in Figures 17(a) and (b). The small duty-cycle, given by the ultrashort pulse-width and the relatively low repetition rate, allowed for a very high peak power (around 9.8 W per

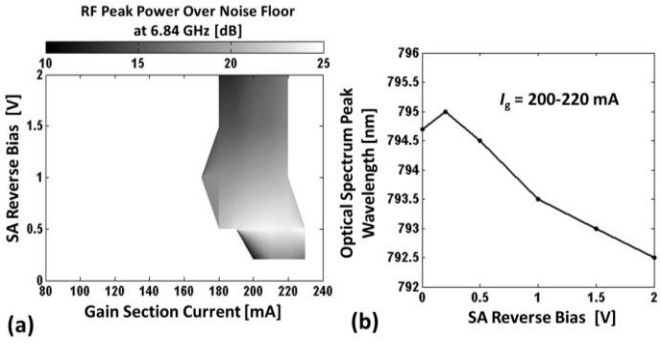


Fig. 15. Map of RF peak power (a) and RF peak frequency (b), as function of gain section current and SA reverse voltage for the 795 nm mode locked laser with a 227 μm long SA at one facet.

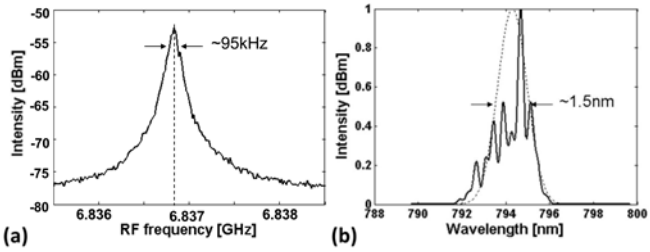


Fig. 16. RF (left) and optical (right) spectra for the laser under best ML conditions ($I_g$ = 210 mA and $V_{SA}$ = 0.5 V).

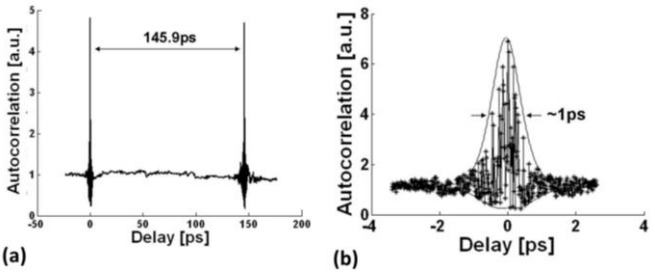


Fig. 17. TPA autocorrelation trace showing (left) the period of pulses and (right) the width of the pulses in the time domain.

facet, for an average power of 48 mW) to be achieved.

## VI. Conclusions

The overall approach for increasing the output power in our devices is the use of epilayer structures with higher $d/\Gamma$, aimed at overcoming the thermal and nonlinear issues typically encountered in high power semiconductor ridge waveguide and broad stripe lasers. A double QW GRINSCH material operating at 830 nm with $d/\Gamma$ ratio of 0.5 μm and a single QW GRINSCH material operating at 795 nm with a $d/\Gamma$ ratio of 0.753 μm were compared. The high $d/\Gamma$ ratio of these laser materials is designed to give better suppression of higher order transverse modes, combined with an increase in the kink-free

output power, by reducing the modal gain per unit length, which thus distributes the gain and thermal dissipation over longer cavities, and by reducing the power density at the facets, giving improved COMD power levels. In this work, mode locking operation in such material structures with higher $d/\Gamma$ ratio, achieved by placing an optical trap in the lower cladding, was investigated for the first time.

CPM operation was demonstrated in 3.7 mm long ML devices at 830 nm. For this geometry, the effect of 150 µm long NAMs was also investigated. It was found that a 40% improvement in the COMD power (70 mW) was seen in devices with NAMs, but with a degraded slope efficiency. Under ML operation, the output power was limited by damage of the SA, due to the high photocurrent produced in the SA itself. This resulted in a lower ML power in the devices with NAMs. However, it was found that NAMs also affect the ML operation, forcing an increase in steady-state gain and gain bandwidth in the forward biased section. As a result, shorter pulses were achieved with NAMs (1.8 ps compared to 2 ps pulses without NAMs), with a higher and narrower RF peak. Better performance was achieved in 5.69 mm long ML devices in the 795 nm material structure. A COMD-free output power of 93 mW was measured with all contacts forward biased. An improved COMD performance was obtained for the 795 nm lasers compared to the 830 nm devices, thanks to their having a 1.7 times larger active mode area, which lowers power the density at the facet, and to their smaller number of wells. This also allowed for improved power performance in the ML regime, where the highest average power was 48 mW, around 1.7 times higher than that measured for the 830 nm devices. Under the optimum ML conditions, pulses as short as 0.71 ps with peak powers of around 9.8 W per facet were generated. The smaller number of wells in the 795 nm devices is believed to shorten the pulses (as also suggested in [8]) and increase the threshold for optical damage (lower absorption at the facets and in the SA). Moreover, the benefits of the larger mode size of the 795 nm lasers in shortening the pulses and suppressing the occurrence of COMD and COSAD are reduced somewhat by the non-CPM cavity design. The 830 nm lasers employ a CPM configuration which promotes pulse shortening thanks to the collision of pulses in the SA [8]. The CPM design also physically separates the SA from the facets (both SA and facets are sources of heat), increasing the threshold for optical damage in such regions. However, although the 830 nm device employs a superior cavity design (CPM), the 795 nm lasers show shorter pulse durations and no COMD or COSAD at higher power levels, thanks to both the larger mode size and smaller number of wells.

In conclusion, our peak power of 9.8 W is very close to the record value (15 W) [23] reported from a QD gain-guided/tapered ML device, with facets coated with antireflection/high reflection films. Our result thus represents, to the best of our knowledge, the highest peak power achieved from any monolithic passively mode locked semiconductor laser with a fundamentally single-transverse mode waveguide and the power would be increased further by coating the facets. Single-transverse mode operation improves fiber coupling efficiency, delivers better beam quality and lower power consumption compared to the gain-guided/tapered devices described in [24], offers better control over material properties compared to QD epistructures and is more resistant to back-reflections.

## REFERENCES


[1] D. Novak, Z. Ahmed, R. B. Waterhouse, and R. S. Tucker. "Signal generation using pulsed semiconductor lasers for application in millimeter-wave wireless links". *IEEE Trans. on Microwave Theory and Techniques*, vol. 43, no. 9, pp. 2257-2262, 1995.

[2] M. Kuramoto *et al.* "Two-photon fluorescence bioimaging with an all semiconductor laser picosecond pulse source". *Opt. Lett.*, vol. 32, no. 18, pp. 2726-2728, Sep. 2007.

[3] J. F. Martins-Filho, C. N. Ironside, and J. S. Roberts. "Quantum well AlGaAs/GaAs monolithic colliding pulse modelocked laser". *Electron. Lett.*, vol. 29, no. 12, pp. 1135-1136, 1993.

[4] D. A. Yanson *et al.*, "Terahertz repetition frequencies from harmonic mode-locked monolithic compound-cavity laser diodes". *App. Phys. Lett.*, vol. 78, no. 23, pp. 3571-3573, 2001.

[5] M. Passerini, M. Sorel, P. J. Laybourn, G. Giuliani, S. Donati. "Fabrication, optimization, and characterization of monolithic semiconductor mode-locked lasers and colliding-pulse mode-locked lasers at millimeterwave frequencies". *Microwave and Terahertz Photonics*, vol. 5466, pp. 116-122, 2004.

[6] I. H. White, M. Xia, and R. V. Penty. "Ultra-short optical pulse generation by InGaAs quantum-dot diode emitters". *22nd IEEE International Semiconductor Laser Conference*, pp. 168-169, 2010.

[7] F. R. Ahmad and F. Rana. "Fundamental and subharmonic hybrid modelocking of a high-power (220 mw) monolithic semiconductor laser". *IEEE Phot. Technol. Lett*., vol. 20, no. 15, pp. 1308-1310, 2008.

[8] M. G. Thompson K. A. Williams and I. H. White. "Long-wavelength monolithic mode-locked diode lasers". *New Journal of Physics*, vol. 6, p. 179, Nov. 2004.

[9] K. Y. Lau and J. Paslaski. "Condition for short pulse generation in ultrahigh frequency mode-locking of semiconductor lasers". *IEEE Phot. Technol. Lett.*, vol. 3, no. 11, pp. 974-976, Nov. 1991.

[10] J. Palaski and K. Y. Lau. "Parameter ranges for ultrahigh frequency mode locking of semiconductor lasers". *App. Phys. Lett.*, vol. 59, no. 1, pp. 7-9, Jul. 1991.

[11] G. P. Agrawal and N. A. Olsson. "Self-phase modulation and spectral broadening of optical pulses in semiconductor laser amplifiers". *IEEE J. Quant. Electron.*, vol. 25, no. 11, pp. 2297-2306, Nov. 1989.

[12] F. R. Ahmad and F. Rana. "Fundamental and subharmonic hybrid mode-locking of a high-power (220 mW) monolithic semiconductor laser", *IEEE Photon. Technol. Lett.*, vol. 20, no. 15, Aug. 2008.

[13] F. R. Ahmad and F. Rana. "Passively mode-locked high-power (210 mW) semiconductor lasers at 1.55-um Wavelength", *IEEE Phot. Technol. Lett.*, vol. 20, no. 3, pp. 190-192, Feb. 2008.

[14] F. R. Ahmad and F. Rana. "High power (150 mW) electrically pumped semiconductor modelocked lasers at 1550 nm with pulse widths approaching 6 ps". *IEEE LEOS Summer Topical Meetings*, pp. 163-164, 2007.

[15] MIT`s Lincoln Laboratory. "Mode-locked semiconductor laser sets power record", *Photonics Spectra*, Mar. 2006. Available: http://www.photonics.com/Article.aspx?AID=24588.

[16] Y. C. Xin, Y. Li, V. Kovanis, A. L. Gray, L. Zhang, and L. F. Lester. "Reconfigurable quantum dot monolithic multisection passive mode-locked lasers". *Optics Express*, vol. 15, no. 12, pp. 7623-7633, Jun. 2007.

[17] A. L. Gray *et al.*, "High-power low-jitter quantum-dot passively mode-locked lasers". vol. 6115, pp. 611502-611508, Feb. 2006.

[18] A. Gubenko *et al.*, "High-power monolithic passively modelocked quantum-dot laser". *Electron. Lett.*, vol. 41, no. 20, pp. 1124-1125, 2005.

[19] M. A. Cataluna E. U. Rafailov and W. Sibbett. "Mode-locked quantum-dot lasers". *Nature Photonics*, vol. 1, pp. 395-401, 2007.

[20] M. G. Thompson, A. R. Rae, Mo Xia, R.V. Penty, and I. H. White. "InGaAs Quantum-Dot Mode-Locked Laser Diodes". *IEEE J. Select. Top. Quant. Electron.*, vol. 15, no. 3, pp. 661-672, 2009.

[21] M. G. Thompson *et al.,* "Subpicosecond high-power mode locking using flared waveguide monolithic quantum-dot lasers". *App. Phys. Lett.,* vol. 88, no. 13, Mar. 2006.

[22] D. Nikitichev *et al.,* "High-power passively modelocked tapered InAs/GaAs quantum-dot lasers". *App. Phys. B: Lasers and Optics*, vol.103, no. 3, pp. 609-613, 2010.

[23] I. H. White, M. Xia, and R. V. Penty. "Ultra-short optical pulse generation by InGaAs quantum-dot diode emitters". *22nd IEEE International Semiconductor Laser Conference*, pp. 168-169, 2010.

[24] D. Nikitichev *et al*., "Passively mode-locked monolithic two-section gain-guided tapered quantum-dot lasers: II. Record 15 Watt peak power generation", *IEEE Conference on Lasers and Electro-Optics Europe 12th European Quantum Electronics Conference (CLEO EUROPE/EQEC)*, May 2011.

[25] A. Akrout *et al.,* "Ultra high repetition rate and very low noise mode locked lasers based on InAs/InP quantum dash active material". *IEEE International Conference on Indium Phosphide Related Materials*, pp. 45-47, May 2009.

[26] K. Merghem *et al.,* "Pulse generation at 346 GHz using a passively mode locked quantum dash-based laser at 1.55 um". *App. Phys. Lett.*, vol. 94, no. 2, pp. 021107-3, Jan. 2009.

[27] B. Qiu, S. D. McDougall, X. Liu, G. Bacchin, and J. H. Marsh. "Design and Fabrication of Low Beam Divergence and High Kink-Free Power Lasers". *IEEE J. Quant. Electron.*, vol. 41, no. 9, pp. 1124-1130, 2005.

[28] I. B. Petrescu-Prahova *et al.,* "High d/gamma values in diode laser structures for very high power". *Proceedings of the SPIE*, vol. 7198, pp. 1I7-1I8, 2009.

[29] B. C. Qiu *et al.,* "Very large arrays of individually addressable, high power, single mode laser arrays in the 800-1000nm wavelength range obtained by quantum well intermixing techniques". *Proceedings of SPIE*, vol. 5738, pp. 33-39, 2005.

[30] C. S. Harder, L. Brovelli, H. P. Meier, and A. Oosenbrug. "High reliability 980-nm pump lasers for Er amplifiers". *Conference on Optical Fiber Communication*, p. 350, Feb. 1997.

[31] S. D. Mc Dougall and C. N. Ironside, "Measurements of reverse and forward bias absorption and gain spectra in semiconductor laser material", *Electron. Lett.*, vol. 31, pp. 2179-2181, 1995.

[32] J. Jimenez. "Laser diode reliability: crystal defects and degradation modes". *Comptes Rendus Physique*, vol. 4, no. 6, pp. 663-673, 2003.

[33] C. L.Walker, A. C. Bryce, and J. H. Marsh. "Improved catastrophic optical damage level from laser with nonabsorbing mirrors". *IEEE Photon. Technol. Lett.*, vol. 14, no. 10, pp. 1394-1396, Oct. 2002.

[34] G. Tandoi, C. N. Ironside and A. C. Bryce. "Nonabsorbing Mirrors for Quantum-Well Colliding Pulse Mode-Locked Lasers". *IEEE Phot. Technol. Lett.*, vol. 23, no. 5, pp. 293-295, 2011.

[35] F. R. Laughton, J. H. Marsh, D. A. Barrow, and E. L. Portnoi, "The two-photon absorption semiconductor waveguide autocorrelator", *IEEE J. Quant. Electron.*, vol. 30, no. 3, Mar. 1994.

[36] F. Camacho *et al.,* "Improvements in mode-locked semiconductor diode lasers using monolithically integrated passive waveguides made by quantum-well intermixing". *IEEE Phot. Technol. Lett.*, vol. 9, no. 9, pp. 1208-1210, 1997.

[37] F. Kefelian, S. O'Donoghue, M. T. Todaro, J. G. McInerney, and G. Huyet. "RF linewidth in monolithic passively mode-locked semiconductor laser". *IEEE Phot. Technol. Lett.*, vol. 20, no. 16, pp. 1405-1407, Aug. 2008.

[38] J. Javaloyes and S. Balle. "Mode-locking in semiconductor Fabry-Perot lasers". *IEEE J. Quant. Electron.*, vol. 46, no. 7, pp. 1023-1030, 2010.

[39] Y. Varshni. "Temperature dependence of the energy gap in semiconductors", *Physica*, vol. 34, pp. 149-154, 1967.

[40] J. W. Tomm and I. Esquivias. "Mirror heating and COD in high-power lasers", *Brighter Meeting*, Lund University, Sweden, Jun. 27-29, 2007. Available: http://www.ist-brighter.eu/tuto3/CONF03/CONF03.pdf.

[41] C. H. Henry, P. M. Petroff, R. A. Logan, and F. R. Merritt. "Catastrophic damage of $Al_xGa_{1-x}As$ double-heterostructure laser material", *J. of App. Phys.*, vol. 50, no. 5, pp. 3721-3732, 1979.


**Giuseppe Tandoi** was born in Bari, Italy, in 1984. He received the M.Sc. degree in Optoelectronics Systems from the Electrical and Electronics Engineering Department at the Politecnico di Bari, Bari, Italy, in 2007. He then worked on the design lateral gratings for distributed feedback quantum cascade lasers operating at 3.34 μm work in collaboration with the School of Engineering at the University of Glasgow. He received his Ph.D. degree in 2010 from the School of Engineering of the University of Glasgow, UK, for its work on monolithic high power passively mode locked GaAs/AlGaAs quantum well lasers.

He is currently working on the integration of optoelectronic devices with gas-filled hollow core fibres for the development of miniature atomic clocks and room temperature magnetometers at the School of Engineering of the University of Glasgow, UK, in collaboration with the National Physical Laboratory, London, UK.

**Charles N. Ironside** (M'87–SM'05) has been in the School of Engineering, University of Glasgow, Glasgow, UK, since 1984. He has been engaged in a variety of optoelectronic projects that include, ultrafast all-optical switching in semiconductor waveguides, monolithic mode-locked semiconductor lasers, broad-band semiconductor lasers, quantum-cascade lasers, and optoelectronic integrated chip (OEIC) devices, which concentrated on the integration of resonant tunnelling diodes with electroabsorption modulators and semiconductor lasers.

**John Marsh** is Head of the School of Engineering and Professor of Optoelectronic Systems at the University of Glasgow. He has wide experience of semiconductor laser technology and integrated optics ranging from epitaxial growth through to the design and development of integrated laser modules for applications including advanced printing and imaging. His work has included research into the fundamental electrical and optical properties of semiconductors, development of novel optoelectronic devices, processes for creating photonic integrated circuits, integrated mode-locked lasers for ultra-short pulse generation, and development and manufacturing of high-power laser array products. He co-founded Intense Ltd in 2000.

He is a Fellow of the Royal Academy of Engineering, Royal Society of Edinburgh, IEEE, IET, Institute of Physics and Royal Society of Arts. He was awarded the 2006 IEEE/LEOS Engineering Achievement Award with Catrina Bryce 'for extensive development and commercialization of quantum well intermixing for photonic devices'. He was also awarded the 2006 IEEE/LEOS Distinguished Service Award 'for major contributions to LEOS governance and for leadership in promoting the development of LEOS as a global society'. He was President of the IEEE Photonics Society in 2008 - 2009.

**A. Catrina Bryce** (M'91–SM'99–F'08) holds the appointment of Professorial Research Fellow in the School of Engineering, University of Glasgow. She has worked in III-V semiconductor optoelectronics for over 20 years. Her research interests include photonic integration, mode-locked diode lasers and high power diode lasers. She has developed techniques for quantum well intermixing and applied these to demonstrate photonic integrated circuits.

Dr. Bryce is a fellow of the Optical Society of America. She was the co-recipient of the 2006 LEOS Engineering Achievement Award for her work on quantum well intermixing. She is an associate editor of the Journal of Quantum Electronics and is the 2013 General co-chair of CLEO: Science and Innovations.